Alkali-metal/alkaline-earth-metal fluorine beryllium borate NaSr3Be3B3O9F4 with large nonlinear optical properties in the deep-ultraviolet region

A. H. Reshak, Hongwei Huang, H. Kamarudin, and S. Auluck

Citation: Journal of Applied Physics **117**, 085703 (2015); doi: 10.1063/1.4913693
View online: http://dx.doi.org/10.1063/1.4913693
View Table of Contents: http://scitation.aip.org/content/aip/journal/jap/117/8?ver=pdfcov
Published by the AIP Publishing

JOURNAL OF APPLIED PHYSICS **117**, 085703 (2015)

Alkali-metal/alkaline-earth-metal fluorine beryllium borate $NaSr_3Be_3B_3O_9F_4$ with large nonlinear optical properties in the deep-ultraviolet region

A. H. Reshak,[1,2,a] Hongwei Huang,[3] H. Kamarudin,[2] and S. Auluck[4]
[1]*New Technologies—Research Centre, University of West Bohemia, Univerzitni 8, 306 14 Pilsen, Czech Republic*
[2]*Center of Excellence Geopolymer and Green Technology, School of Material Engineering, University Malaysia Perlis, 01007 Kangar, Perlis, Malaysia*
[3]*School of Materials Science and Technology, China University of Geosciences, Beijing 100083, People's Republic of China*
[4]*Council of Scientific and Industrial Research—National Physical Laboratory, Dr. K S Krishnan Marg, New Delhi 110012, India and Physics Department, Indian Institute of Technology - Delhi, Hauz Khas, New Delhi 110016, India*

(Received 17 November 2014; accepted 16 February 2015; published online 25 February 2015)

The linear optical response and second harmonic generation (SHG) in alkali-metal/alkaline-earth-metal fluorine beryllium borate $NaSr_3Be_3B_3O_9F_4$ are investigated by means of density functional theory. Calculations are performed using four types of exchange correlations: Ceperley-Alder local density approximation, Perdew Burke and Ernzerhof general gradient approximation, Engel-Vosko generalized gradient approximation, and the recently modified Becke-Johnson potential (mBJ). The mBJ approach brings the calculated band gap (7.20 eV) in excellent agreement with the experimental one (7.28 eV). The calculated values of the uniaxial anisotropy $\delta\varepsilon = -0.076$ and the birefringence $\Delta n(0) = 0.052$ indicate considerable anisotropy in the linear optical properties, which makes it favorable for the second harmonic generation. The dominant component of the second harmonic generation is $\chi^{(2)}_{111}(\omega)$. The value of $|\chi^{(2)}_{111}(\omega)|$ is about 1.2 pm/V at $\lambda = 1064$ nm in agreement with previous calculations. To analyze the origin of the high SHG of $NaSr_3Be_3B_3O_9F_4$ single crystals, we have correlated the features of $|\chi^{(2)}_{111}(\omega)|$ spectra with the features of $\varepsilon_2(\omega)$ spectra as a function of $\omega/2$ and ω. From the calculated dominant component $|\chi^{(2)}_{111}(\omega)|$, we find that the microscopic first hyperpolarizability, β_{111}, the vector components along the dipole moment direction is 0.5×10^{-30} esu at static limit and 0.6×10^{-30} esu at $\lambda = 1064$ nm. © *2015 AIP Publishing LLC*.
[http://dx.doi.org/10.1063/1.4913693]

I. INTRODUCTION

Borate crystals compared to the well known inorganic compounds[1] exhibit promising features which make them useful in numerous applications in laser and nonlinear optics. Owing to their ultraviolet (UV) transparency, borate crystals play a very important role in the UV application. Also, they exhibit high damage threshold for laser radiation. In the recent years, the borate crystals have been extensively investigated and several promising crystals were found, namely, $CsLiB_6O_{10}$,[2] BiB_3O_6,[3–6] BaB_2O_4,[7] LiB_3O_5,[8] CsB_3O_5,[9] $La_2CaB_{10}O_{19}$.[10] These crystals exhibit high nonlinear optical properties (NLO) in the UV and visible region. However, none of these crystals is able to generate deep-UV radiation. Therefore, extensive investigations were carried out by several workers for new deep-UV NLO crystals.[11–15] Huang *et al.*[16] report the synthesis of $NaSr_3Be_3B_3O_9F_4$ single crystals which may be a promising NLO material in the deep-UV region. Recently, Wang *et al.*[17] have used the top-seeded solution growth method to grow $NaSr_3Be_3B_3O_9F_4$ single crystals with dimensions up to $13 \times 14 \times 20\,mm^3$. They have measured the energy band gap and the refractive indices.

As there is a dearth of information on the linear, nonlinear optical properties, and the hyperpolarizability of alkali-metal/alkaline-earth-metal fluorine beryllium borate $NaSr_3Be_3B_3O_9F_4$ single crystal, we address ourselves to a comprehensive theoretical calculation based on the density functional theory (DFT) within the state-of-the-art full potential linear augmented plane wave (FPLAPW) method, which has proven to be one of the most accurate methods for the computation of the electronic structure of solids within DFT.[18,19] The optical properties give deep insight into the electronic structures and the physical properties of materials. Therefore, we have calculated the linear, nonlinear optical properties, and the hyperpolarizability of alkali-metal/alkaline-earth-metal fluorine beryllium borate $NaSr_3Be_3B_3O_9F_4$ single crystal. This is a natural extension to previous works.[16,17]

II. DETAILS OF CALCULATIONS

The linear optical response and second harmonic generation (SHG) of alkali-metal/alkaline-earth-metal fluorine beryllium borate $NaSr_3Be_3B_3O_9F_4$ single crystal are investigated by means of DFT. We have employed the state-of-the-art FPLAPW method in a scalar relativistic version as embodied in the WIEN2k code.[20] Different possible approximations for the exchange-correlation potential were used. For instance, we have started the calculations with Ceperley-

[a]Author to whom correspondence should be addressed. Electronic mail: maalidph@yahoo.com. Tel.: +420 777729583, Fax. +420-386 361255

Alder local density approximation (CA-LDA)[21] and Perdew, Burke, and Ernzerhof generalized gradient approximation (PBE-GGA),[22] which is based on exchange-correlation energy optimization to calculate the total energy. As is well known, band gaps are underestimated in LDA and GGA. To overcome this drawback, we have used the Engel-Vosko generalized gradient approximation (EV-GGA).[23] We find that the value of the band gap is significantly enhanced to be 6.20 eV but still below the experimental value (7.28 eV)[16,17] by about 1.08 eV. Therefore, we applied the recently modified Becke-Johnson potential (mBJ)[24] which brings the energy gap (7.20 eV) very close to the experimental one. The modified Becke-Johnson potential allows the calculation of band gaps with accuracy similar to the very expensive GW calculations.[24] It is a local approximation to an atomic "exact-exchange" potential together with a screening term. The atomic positions obtained from the X-ray diffraction data (XRD) data are optimized by minimizing the forces acting on each atom using GGA-PBE. We assume that the structure is totally relaxed when the forces on each atom reach values less than 1 mRy/a.u. The Kohn-Sham equations are solved using a basis of linear APWs. The potential and charge density in the muffin-tin spheres are expanded in spherical harmonics with $l_{max}=8$ and nonspherical components up to $l_{max}=6$. In the interstitial region, the potential and the charge density are represented by Fourier series. Self-consistency is obtained using 300 $\vec{k}$ points in the irreducible Brillouin zone (IBZ). The linear optical susceptibilities were calculated using 800 $\vec{k}$ points, whereas for the nonlinear optical susceptibilities, we used 1800 $\vec{k}$ points in the IBZ.

III. RESULTS AND DISCUSSION

A. Linear optical response

The alkali-metal/alkaline-earth-metal fluorine beryllium borate $NaSr_3Be_3B_3O_9F_4$ single crystal crystallizes in the non-centrosymmetric trigonal space group R*3m*.[16] Hence, two components of the optical dielectric tensor components completely define the linear optical susceptibilities. These are the imaginary parts $\varepsilon_2^{xx}(\omega)=\varepsilon_2^{yy}(\omega)$ and $\varepsilon_2^{zz}(\omega)$ of the dielectric tensor. The imaginary parts can be calculated using the following expression:

$$\varepsilon_2^{ij}(\omega)=\frac{8\pi^2\hbar^2e^2}{m^2V}\sum_k\sum_{cv}(f_c-f_v)\frac{p_{cv}^i(k)p_{vc}^j(k)}{E_{vc}^2}\times\delta[E_c(k)-E_v(k)-\hbar\omega]. \quad (1)$$

This expression is taken from Ref. 25, where m, e, and $\hbar$ are the electron mass, charge, and Planck's constant, respectively. f_c and f_v represent the Fermi distributions of the conduction and valence bands, respectively. The term $p_{cv}^i(k)$ denotes the momentum matrix element transition from the energy level c of the conduction band to the level v of the valence band at certain **k**-point in the IBZ and V is the unit cell volume. According to the dipolar selection rule, only transitions changing the angular momentum quantum number l by unity are allowed.

As borate $NaSr_3Be_3B_3O_9F_4$ single crystals possess a wide direct energy band gap (7.20 eV), it is expected to be an active optical material suitable for deep ultraviolet optical applications. The optical functions are calculated using four types of exchange correlation potentials (CA-LDA, PBE-GGA, EV-GGA, and mBJ). We find that only mBJ approach brings the energy gap in excellent agreement with the experimental one, therefore we represent only the results obtained by the mBJ approach. The imaginary part of the optical function's dispersion for different incident light polarizations [1 0 0] and [0 0 1] with respect to the crystalline axes is illustrated in Fig. 1(a). The absorption edges (optical gap) for $\varepsilon_2^{xx}(\omega)$ along the polarizations direction [1 0 0] and $\varepsilon_2^{zz}(\omega)$ along the polarizations direction [0 0 1] are located at 7.20 eV. There exists a strong anisotropy among the two polarization directions [1 0 0] and [0 0 1]. It is well know that the anisotropy in the linear optical susceptibilities is favorable to enhancing the second harmonic generation. The perpendicular component $\varepsilon_2^{xx}(\omega)$ exhibits a main peak around 10.0 eV situated between small humps distributed on the left and right hand shoulders. The main peak of the parallel component $\varepsilon_2^{zz}(\omega)$ is located around 11.0 eV and presents insignificant hump on the left hand shoulder and two significant humps on the right hand shoulder. The main peaks of $\varepsilon_2^{xx}(\omega)$ and $\varepsilon_2^{zz}(\omega)$ occur due to the transitions from Sr-s/p, Na-s/p, Be-s/p, B-s/p, F1/F2-s/p, and O1/O1-s to Sr-s/p/d, Na-s/p, Be-s/p, B-s/p, F1/F2-s/p, and O1/O1-s/p.

From the imaginary part, one can obtain the real part $\varepsilon_1^{xx}(\omega)$ and $\varepsilon_1^{zz}(\omega)$ of optical function's dispersion for different incident light polarizations [1 0 0] and [0 0 1] with respect to the crystalline axes by means of Kramers-Kronig transformation.[26] $\varepsilon_1^{xx}(\omega)$ and $\varepsilon_1^{zz}(\omega)$ are illustrated in Fig. 1(b), which shows again a considerable anisotropy between [1 0 0] and [0 0 1] polarization directions. The values of $\varepsilon_1^{xx}(0)$ and $\varepsilon_1^{zz}(0)$ are listed in Table I. We have calculated the uniaxial anisotropy $\delta\varepsilon=[(\varepsilon_0^{II}-\varepsilon_0^{\perp})/\varepsilon_0^{tot}]$ which is about -0.076, indicating the existence of the considerable anisotropy between the two polarization directions. Thus, $NaSr_3Be_3B_3O_9F_4$ is a negative uniaxial crystal in agreement with the recent work of Wang *et al.*[17] and Huang *et al.*[16]

From the imaginary and real parts of the optical function, we can evaluate the refractive indices $n(\omega)$, birefringence $\Delta n(\omega)$, absorption coefficient $I(\omega)$, and reflectivity $R(\omega)$. The calculated refractive indices $n^{xx}(\omega)$ and $n^{zz}(\omega)$ as represented in Fig. 1(c) exhibit high values at low energies which reach its maximum peak between 7.5 and 8.5 eV then drop to lower value. The two components of the refractive indices exhibit strong anisotropy between the two polarization directions. Using the existence information of the refractive indices, the birefringence $(\Delta n(\omega)=n^{xx}(\omega)-n^{zz}(\omega))$ can be obtained. The obtained values of the birefringence and the corresponding refractive indices at the static limit are listed in Table I, along with the previously calculated and measured values,[16,17] good agreement is found. Furthermore, we should emphasize that previously we have performed similar calculations on several compounds using CA-LDA, PBE-GGA, and EV-GGA, and found that the calculated refractive indices are in good agreement with experiment. In our previous work on $KTiOPO_4$ (KTP)[27] $BaBiBO_4$,[28]

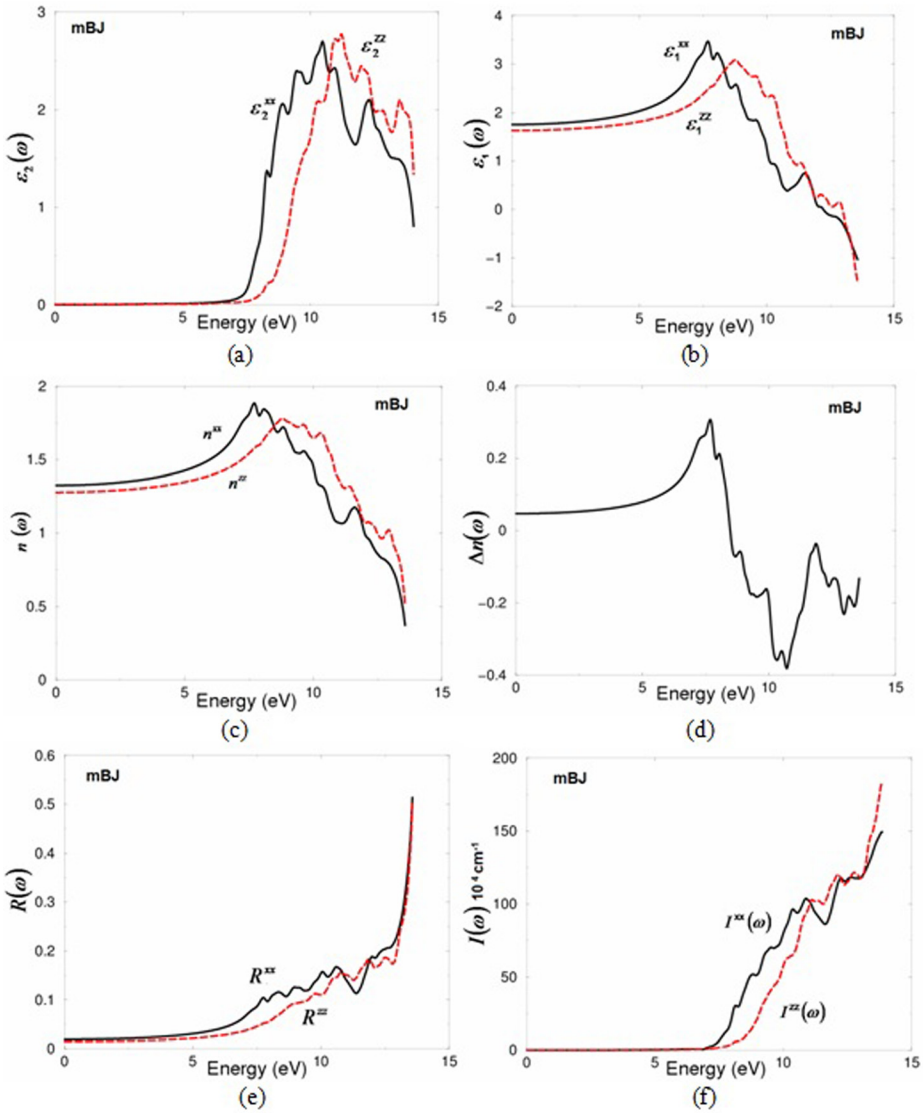

FIG. 1. (a) Calculated $\varepsilon_2^{xx}(\omega)$ (dark solid curve-black) and $\varepsilon_2^{zz}(\omega)$ (light dashed curve-red); (b) calculated $\varepsilon_1^{xx}(\omega)$ (dark solid curve-black) and $\varepsilon_1^{zz}(\omega)$ (light dashed curve-red); (c) calculated refractive indices $n^{xx}(\omega)$ (dark solid curve-black) and $n^{zz}(\omega)$ (light dashed curve-red); (d) calculated birefringence $\Delta n(\omega)$; (e) calculated $R^{xx}(\omega)$ (dark solid curve-black) and $R^{zz}(\omega)$ (light dashed curve-red) of reflectivity spectra; (f) calculated absorption coefficient $I^{xx}(\omega)$ (dark solid curve-back) and $I^{zz}(\omega)$ (light dashed curve-red), the absorption coefficient in $10^4\,\mathrm{cm}^{-1}$.

TABLE I. The calculated energy band gap in comparison with the experimental value, $\varepsilon_1^{xx}(0)$, $\varepsilon_1^{yy}(0)$, $\varepsilon_1^{zz}(0)$, $\varepsilon_1^{average}(0)$, $n^{xx}(0)$, $n^{yy}(0)$, $n^{zz}(0)$, $n^{average}(0)$, and $\Delta n(0)$ without and with scissors corrections.

	LDA	GGA	EVGGA	mBJ	Experimental
Eg	4.82	5.16	6.20	7.20	7.28 [a,b] (absorption edge = 170 nm)[a,b]
$\varepsilon_1^{xx}(0)$	2.06	1.97	1.85	1.76	…
$\varepsilon_1^{zz}(0)$	1.93	1.85	1.74	1.63	
$\varepsilon_1^{average}(0)$	1.995	1.910	1.795	1.695	…
$n^{xx}(0)$	1.435	1.405	1.376	1.329	1.592 at $\lambda = 852$ nm[b]
$n^{zz}(0)$	1.391	1.361	1.331	1.277	1.534 at $\lambda = 852$ nm[b]
$\Delta n(0)$	0.044	0.044	0.045	0.052	0.056 at $\lambda = 800$ nm[a] 0.057 at $\lambda = 852$ nm[b]

[a]Reference 16.
[b]Reference 17.

$Na_3La9O_3(BO_3)_8$,[29] BiB_3O_6,[30] $CuInX_2$ (X = S, Se, Te),[31] and $LiGaX_2$ (X = S, Se),[32] we have compared the calculated refractive indices and birefringence with experiment data and found very good agreement. For instance, we have compared our calculated $\Delta n(\omega)$ at $\lambda = 1064$ nm for $KTiOPO_4$ (Ref. 27) which is about 0.074 with the experimental value of $\Delta n(\omega) = 0.083$ at $\lambda = 1064$ nm for $KTiOPO_4$. Therefore, the present calculation obtained using mBJ is expected to be close to the experimental values. Fig. 1(d) shows the reflectivity spectra of $NaSr_3Be_3B_3O_9F_4$. At low energies between 0.0 up to 7.0 eV, the crystal shows a very low reflectivity then rapidly increases with increasing the energy of the incident photons. The two components of the absorption coefficient illustrated in Fig. 1(e) indicate that the absorption edge occurs at 7.20 eV which confirms that the crystal under investigation is suitable for deep ultraviolet applications.

B. Second harmonic generation

Since $NaSr_3Be_3B_3O_9F_4$ single crystal crystallizes in the non-centrosymmetric trigonal space group R3*m*, therefore there are only three nonzero complex second-order nonlinear optical susceptibility tensors $\chi^{(2)}_{111}(-2\omega;\omega;\omega) = -\chi^{(2)}_{122}(-2\omega;\omega;\omega)$ $\chi^{(2)}_{333}(-2\omega;\omega;\omega)$. The formulae of the complex second-order nonlinear optical susceptibility tensor $\chi^{(2)}_{ijk}(-2\omega;\omega;\omega)$ can be found somewhere else.[33–36] We have calculated these three components using CA-LDA, PBE-

GGA, EV-GGA, and mBJ. Since mBJ brings the calculated energy gap very close to the experimental one, therefore we will present the results obtained by mBJ. It is well known that the nonlinear optical properties are very sensitive to the energy band gap's value,[27–32] thus in addition to mBJ approach, we introduce a quasi particle self-energy corrections at the level of scissors operators in which the energy bands are rigidly shifted to merely bring the calculated energy gap closer to the experimental gap. Fig. 2(a) illustrates the absolute values of $|\chi^{(2)}_{111}(\omega)|$ and $|\chi^{(2)}_{333}(\omega)|$. It is clear that $|\chi^{(2)}_{111}(\omega)|$ shows the highest value so as to act as the dominant component with value of about 1.1 pm/V in the static limit and 1.2 pm/V at $\lambda = 1064$ nm in agreement with the previous calculated value 1.32 pm/V.[16] This is comparable to the experimental value of the well known $KTiOPO_4$ single crystals which exhibits a SHG value of about 1.19 ± 0.08 pm/V (Ref. 37) and 1.91 ± 0.2 pm/V (Ref. 38) for the $|\chi^{(2)}_{113}(\omega)|$ component. Thus, the $NaSr_3Be_3B_3O_9F_4$ single crystals can serve as a promising NLO material. In Fig. 2(b), we represent the dispersions of imaginary and real parts of the dominant component $\chi^{(2)}_{111}(-2\omega;\omega;\omega)$. One can clearly see that the imaginary part of $\chi^{(2)}_{111}(-2\omega;\omega;\omega)$ component is zero below the half band gap ($E_g/2$). We should emphasize that at above $E_g/2$ the 2 ω resonance starts to contribute,[34,36] and at above the fundamental value of the energy gap (E_g), the ω resonance begins to contribute in addition to 2 ω resonance. Therefore, one can see that the maximum peaks in the imaginary and real parts of $\chi^{(2)}_{111}(-2\omega;\omega;\omega)$ component occur above the value of E_g. Fig. 2(c) depicts the contributions of ω and 2 ω resonances to the total nonlinear optical susceptibilities, it is clear that ω and 2 ω resonances can be further separated into inter-band and intra-band contributions with opposite signs throughout the frequency range. In order to resolve the spectral features of the obtained $\chi^{(2)}_{111}(-2\omega;\omega;\omega)$ component, we have correlated the features of $|\chi^{(2)}_{111}(\omega)|$ spectra with the features of $\varepsilon_2(\omega)$ spectra as a function of $\omega/2$ and ω, see Fig. 2(d). The first structure $|\chi^{(2)}_{111}(\omega)|$ between 3.9 and 7.28 eV is mainly originated from 2 ω resonance [see $\varepsilon_2(\omega/2)$, Fig. 2(d) - lower panel]. The second structure between 7.28 and 10.0 eV is associated with interference between 2 ω and ω resonances (the threshold of $\varepsilon_2(\omega)$) [see $\varepsilon_2(\omega/2)$ and $\varepsilon_2(\omega)$ Fig. 2(d) - lower panel]. The last spectral structure (within 10.0 – 14.0 eV) is mainly due to ω resonance and is associated with the second structure in $\varepsilon_2(\omega)$.

From the calculated $\chi^{(2)}_{ijk}(\omega)$ dispersion, we have obtained the microscopic first hyperpolarizability, β_{ijk}, the vector components along the dipole moment direction. The microscopic first hyperpolarizability terms cumulatively yield a bulk observable second order susceptibility term,

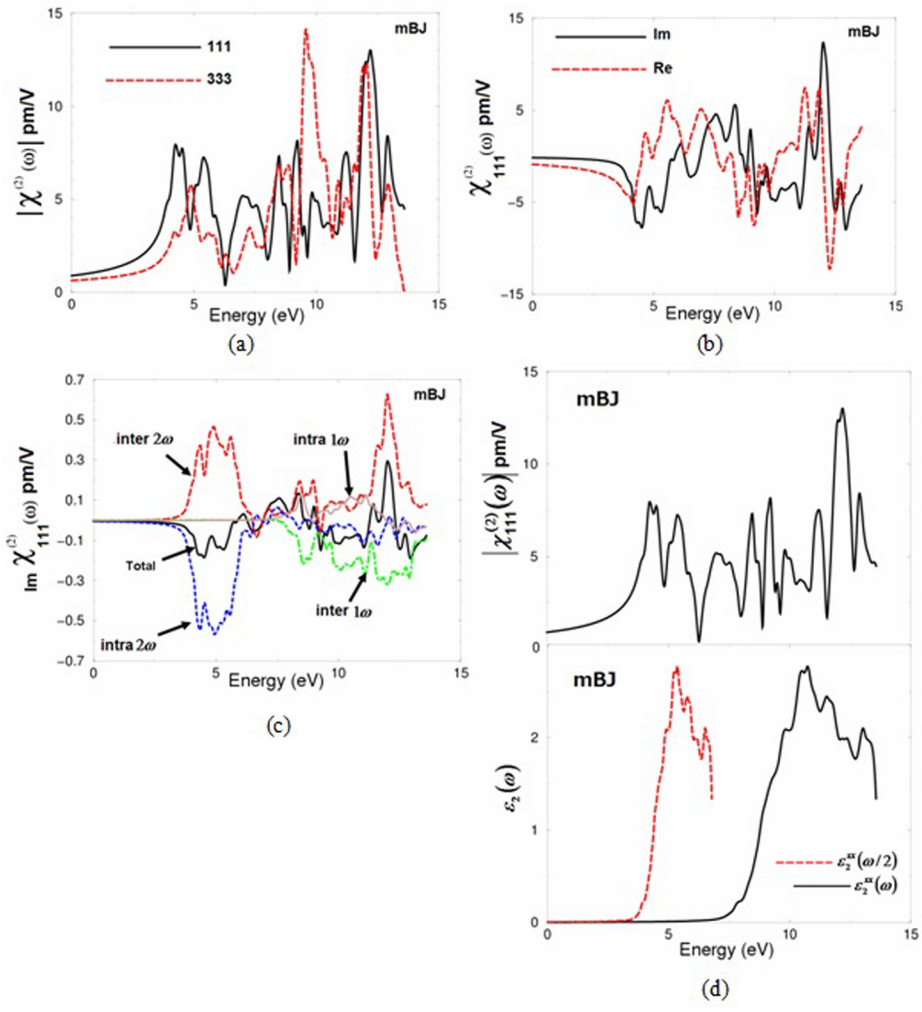

FIG. 2. (a) Calculated $|\chi^{(2)}_{ijk}(\omega)|$ for the two components using mBJ with scissor correction; (b) calculated imaginary $\chi^{(2)}_{111}(\omega)$(dark solid curve-black) and real $\chi^{(2)}_{111}(\omega)$ (light dashed curve-red) spectra, using EV-GGA with scissors correction; (c) calculated imaginary $\chi^{(2)}_{111}(\omega)$ spectrum (dark solid curve-black) along with the intra (2 ω)/(1 ω) (light solid curve-blue)/(light dashed doted curve-cyan) and inter (2 ω)/(1 ω) (light long dashed curve-red)/(light doted curve-green)-band contributions, here all imaginary $\chi^{(2)}_{111}(\omega)$ are multiplied by 10^{-7}, in esu units; (d) *upper panel:* calculated $|\chi^{(2)}_{111}(\omega)|$ (dark solid curve-black) using EV-GGA with scissors correction; *lower panel:* calculated $\varepsilon_2^{xx}(\omega)$ (dark solid curve-black); calculated $\varepsilon_2^{xx}(\omega/2)$ (dark dashed curve-red).

$\chi^{(2)}_{ijk}(\omega)$, which in turn is responsible for the high SHG response.[39–41] For the dominant component $|\chi^{(2)}_{111}(\omega)|$, we have calculated β_{111} at the static limit and at $\lambda = 1064$ nm, the expression for calculating β_{ijk} is given elsewhere.[38] We have found that these values are equal to 0.5×10^{-30} esu at static limit and 0.6×10^{-30} esu at $\lambda = 1064$ nm. We would like to mention here that in our previous works,[27–29,36,42–44] we have calculated the linear and nonlinear optical susceptibilities using FPLAPW method on several systems whose linear and nonlinear optical susceptibilities are known experimentally, in those previous calculations, we found very good agreement with the experimental data. Thus, we believe that our calculations reported in this paper would produce very accurate and reliable results.

IV. CONCLUSIONS

Based on the density functional theory, we have calculated the hyperpolarizability, linear optical response, and second harmonic generation of $NaSr_3Be_3B_3O_9F_4$ single crystals. Calculations were performed using the state-of-the-art FPLAPW method in a scalar relativistic version as embodied in the WIEN2k code with four types of exchange correlation potentials, namely, CA-LDA, PBE-GGA, EV-GGA, and mBJ. We should emphasize that mBJ brings the calculated energy gap (7.20 eV) very close to the experimental one (7.28 eV). We have calculated the imaginary and real parts of the optical function's dispersion for different incident light polarizations [1 0 0] and [0 0 1] with respect to the crystalline axis and found that the optical gap shows close agreement with the experimental one. The values of calculated uniaxial anisotropy $\delta\varepsilon = -0.076$ and the birefringence $\Delta n(0) = 0.052$ indicate considerable anisotropy in the linear optical properties which makes them favorable for the second harmonic generation. These values are in good agreement with the previous results. In addition, the second harmonic generation of $NaSr_3Be_3B_3O_9F_4$ single crystal is calculated using four types of exchange correlation potentials. The investigated crystal possesses three nonzero complex second-order nonlinear optical susceptibility tensors, we found that $|\chi^{(2)}_{111}(\omega)|$ shows the highest value therefore it acts as the dominant component with value of about 1.1 pm/V at static limit and 1.2 pm/V at $\lambda = 1064$ nm which shows that the $NaSr_3Be_3B_3O_9F_4$ single crystals are a promising NLO material being comparable to the well known $KTiOPO_4$ single crystals which exhibit a SHG value of about 1.19 ± 0.08 pm/V and 1.91 ± 0.2 pm/V for the $|\chi^{(2)}_{113}(\omega)|$ component. We have resolved the spectrum of the dominant component $|\chi^{(2)}_{111}(\omega)|$ by correlating the spectral features of $|\chi^{(2)}_{111}(\omega)|$ with the spectral features of $\varepsilon_2(\omega)$ in terms of single photon (ω) and two photon ($\omega/2$) resonances. Finally, we have calculated the value of the first hyperpolarizability, β_{111} of the dominant component and found to be 0.5×10^{-30} esu at static limit and 0.6×10^{-30} esu at $\lambda = 1064$ nm.

ACKNOWLEDGMENTS

The result was developed within the CENTEM project, reg. no. CZ.1.05/2.1.00/03.0088, cofunded by the ERDF as part of the Ministry of Education, Youth and Sports OP RDI programme and, in the follow-up sustainability stage, supported through CENTEM PLUS (LO1402) by financial means from the Ministry of Education, Youth and Sports under the "National Sustainability Programme I." Computational resources were provided by MetaCentrum (LM2010005) and CERIT-SC (CZ.1.05/3.2.00/08.0144) infrastructures. S.A. thanks Council of Scientific and Industrial Research (CSIR) - National Physical Laboratory and Physics Department Indian Institute of Technology, Delhi for financial support.

[1]C. Chen, Y. Wu, and R. Li, J. Cryst. Growth **99**, 790 (1990).
[2]Y. Mori, I. Kuroda, T. Sasaki, and S. Nakai, Jpn. J. Appl. Phys. Part 2 **34**, L296 (1995).
[3]G. Aka, A. Khan-Harari, D. Vivien, J. M. Benitez, F. Salin, and J. Godard, Eur. J. Solid State Inorg. Chem. **33**, 727 (1996).
[4]T. Lukasiewicz, I. V. Kityk, M. Makowskajanusik, A. Majchrowski, Z. Galazka, H. Kaddouri, and Z. Mierczyk, J. Cryst. Growth **237–239**, 641 (2002).
[5]H. Hellwig, J. Liebertz, and L. Bohaty, Solid State Commun. **109**(4), 249 (1998).
[6]M. Ghotbi, M. Ebrahim-Zadeh, A. Majchirowski, E. Michalski, and I. V. Kityk, Opt. Lett. **29**, 2530 (2004).
[7]C. T. Chen, B. C. Wu, A. D. Jiang, and G. M. You, Sci. Sin., Ser. B (Engl. Ed.) **28**, 235 (1985).
[8]C. T. Chen, Y. C. Wu, A. D. Jiang, B. C. Wu, G. M. You, R. K. Li, and S. J. Lin, J. Opt. Soc. Am. B **6**, 616 (1989).
[9]Y. C. Wu, T. Sasaki, S. Nakai, A. Yokotani, H. G. Tang, and C. T. Chen, Appl. Phys. Lett. **62**, 2614 (1993).
[10]Y. Wu, J. Liu, P. Fu, J. Wang, F. Guo, G. Zhao, J. Qin, and C. Chen, Proc. SPIE **3556**, 8 (1998).
[11]S. C. Wang, N. Ye, W. Li, and D. Zhao, J. Am. Chem. Soc. **132**, 8779 (2010).
[12]W. L. Zhang, W. D. Cheng, H. Zhang, L. Geng, C. S. Lin, and Z. Z. He, J. Am. Chem. Soc. **132**, 1508 (2010).
[13]H. P. Wu, S. L. Pan, K. R. Poeppelmeier, H. Y. Li, D. Z. Jia, Z. H. Chen, X. Y. Fan, Y. Yang, J. M. Rondinelli, and H. S. Luo, J. Am. Chem. Soc. **133**, 7786 (2011).
[14]M. C. Chen, L. H. Li, Y. B. Chen, and L. Chen, J. Am. Chem. Soc. **133**, 4617 (2011).
[15]S. F. Jin, G. M. Cai, W. Y. Wang, M. He, S. C. Wang, and X. L. Chen, Angew. Chem. **122**, 5087 (2010); Angew. Chem. Int. Ed. **49**, 4967 (2010).
[16]H. Huang, J. Yao, Z. Lin, X. Wang, R. He, W. Yao, N. Zhai, and C. Chen, Angew. Chem. Int. Ed. **50**, 9141–9144 (2011).
[17]X. Wang, L. Liu, X. Wang, L. Bai, and C. Chen, CrystEngComm **17**, 925 (2015).
[18]S. Gao, Comput. Phys. Commun. **153**, 190 (2003).
[19]K. Schwarz, J. Solid State Chem. **176**, 319 (2003).
[20]P. Blaha, K. Schwarz, G. K. H. Madsen, D. Kvasnicka, and J. Luitz, *WIEN2k, An Augmented Plane Wave Plus Local Orbitals Program for Calculating Crystal Properties* (Vienna University of Technology, Austria, 2001).
[21]W. Kohn and L. J. Sham, Phys. Rev. A **140**, A1133 (1965).
[22]J. P. Perdew, S. Burke, and M. Ernzerhof, Phys. Rev. Lett. **77**, 3865 (1996).
[23]E. Engel and S. H. Vosko, Phys. Rev. B **47**, 13164 (1993).
[24]F. Tran and P. Blaha, Phys. Rev. Lett. **102**, 226401 (2009).
[25]F. Bassani and G. P. Parravicini, *Electronic States and Optical Transitions in Solids* (Pergamon Press Ltd., Oxford, 1975), pp. 149–154.
[26]H. Tributsch, Z. Naturforsch. A **32A**, 972 (1977).
[27]A. H. Reshak, V. Kityk, and S. Auluck, J. Phys. Chem. B **114**, 16705–16712 (2010).
[28]A. H. Reshak, S. Auluck, and I. V. Kityk, J. Solid State Chem. **181**, 789–795 (2008).
[29]A. H. Reshak, S. Auluck, and I. V. Kityk, J. Phys.: Condens. Matter **20**, 145209 (2008).
[30]A. H. Reshak, S. Auluck, and I. V. Kityk, Appl. Phys. A **91**, 451–457 (2008).
[31]A. H. Reshak and S. Auluck, PMC Phys. B **1**, 12 (2008).

[32]A. H. Reshak, S. Auluck, and I. V. Kityk, J. Alloys Compd. **473**, 20 (2009).
[33]S. Sharma, J. K. Dewhurst, and C. Ambrosch-Draxl, Phys. Rev. B **67**, 165332 (2003).
[34]A. H. Reshak, Ph.D. thesis, Indian Institute of Technology-Rookee, India, 2005.
[35]A. H. Reshak, J. Chem. Phys. **125**, 034710 (2006).
[36]A. H. Reshak, J. Chem. Phys. **124**, 104707 (2006).
[37]L. K. Cheng, L. T. Cheng, J. Galperin, P. A. M. Hotsenpiller, and J. D. Bierlein, J. Cryst. Growth **137**, 107 (1994).
[38]H. Vanherzeele and J. D. Bierlein, Opt. Lett. **17**, 982 (1992).
[39]A. H. Reshak, RSC Adv. **4**, 64947 (2014).
[40]R. Y. Boyd, *Principles of Nonlinear Optics* (Academic Press, NY, 1982), p. 420.
[41]R. W. Boyd, *Nonlinear Optics*, 3rd ed. (Academic Press, 2008).
[42]A. H. Reshak, Eur. Phys. J. B **47**, 503–508 (2005).
[43]A. H. Reshak, S. Auluck, D. Stys, I. V. Kityk, H. Kamarudin, J. Berdowski, and Z. Tylczynskif, J. Mater. Chem. **21**, 17219 (2011).
[44]A. H. Reshak, M. Piasecki, S. Auluck, I. V. Kityk, R. Khenata, B. Andriyevsky, C. Cobet, N. Esser, A. Majchrowski, M. S'wirkowicz, R. Diduszko, and W. Szyrski, J. Phys. Chem. B **113**(46), 15237 (2009).